W-Band Vibrometer for Noncontact Thermoacoustic Imaging

Archita Hati[ID] and Craig W. Nelson

Abstract—Noncontact thermoacoustic imaging (TAI) has several desirable characteristics for applications such as explosive detection in high-water-content media. In this letter, we report a detection technique using millimeter-wave interferometry based on sensitive phase detection at W-band. The displacement sensitivity of the proposed W-band vibrometer at 95 GHz is of the order of 1 nm. We also analyze the effect of phase noise on the sensitivity of the vibrometer. Unlike laser-based sensors, a W-band sensor has several advantages; it can easily penetrate surface obscurants such as fur or cloth and it does not require a highly reflective surface of the target to detect the thermoacoustic vibrations.

Index Terms—Phase noise, thermoacoustic imaging (TAI), vibrometer, W-band.

I. INTRODUCTION

MICROWAVE-INDUCED thermoacoustic imaging (TAI) is an emerging imaging technique primarily used for biomedical applications such as early cancer detection [1]–[3]. The main advantage of this technique is that it combines the benefits of high-imaging contrast of microwave imaging [4] and high resolution of ultrasound imaging [5]. In microwave-induced TAI, the desired target is irradiated with short pulses of the high-power microwave signal. The energy absorbed by the target produces heating and thermoelastic expansion which, in turn, generates thermoacoustic vibrations that propagate through the target. These vibrations are then detected at the surface of the target with either contact or noncontact sensors [2], [6]. The TAI systems using transducers (normal ultrasound detection) require contact with the target media to produce detailed internal images of high-water content organs. Noncontact (standoff) TAI has useful features for explosives detection. Optical interferometer techniques for measuring the surface displacement of animal or human organs use photoacoustic imaging (PAI) [7], [8]. Optical vibrometers can operate with detection thresholds at the picometer level [9], but their main drawback is that optical signals cannot penetrate through surface obscurants such as fur or cloth.

Sensitive standoff explosives detection techniques are developed to detect explosives hidden in opaque media with high-water content [10]–[14]. In this letter, we describe a detection technique using millimeter-wave (mm-wave) interferometry based on sensitive phase detection at W-band (up to 110 GHz). We tested the performance of the vibrometer at 95 GHz and measured nanometer-scale surface displacement. The mm-wave vibrometer was also successfully tested with actual samples [10].
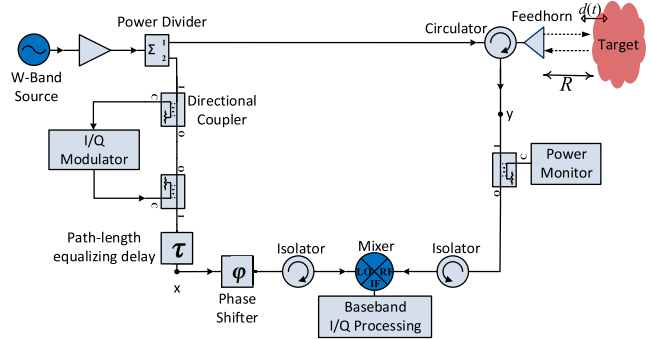
Fig. 1. Block diagram of the single-channel W-band standoff vibrometer.

II. DESCRIPTION OF THE W-BAND VIBROMETER

The block diagram of the single channel W-band vibrometer is shown in Fig. 1. The continuous-wave (CW) signal from the W-band source is incident on the target at a distance R from the transmitter. If the surface of the target experiences time-dependent displacement, $d(t)$, the Doppler shift of the reflected signal can be described as phase modulation, $\theta_d(t)$ and expressed as [3]

$$\theta_d(t) = \frac{2\pi \times 2d(t)}{\lambda} = \frac{4\pi d(t)}{\lambda} \quad (1)$$

where λ is the wavelength of the transmitted signal.

The return signal reflected off the target is then mixed with the reference emitter signal at the mixer. The delay mismatch between these two signals is carefully equalized with path-length delay, τ. If $d(t) \ll \lambda$ and the phase between the local oscillator (LO) and reference frequency (RF) port of the mixer is set to $\pi/2$, the baseband voltage fluctuations at the intermediate frequency (IF) output of the mixer will be proportional to $\theta_d(t)$. As in a conventional phase-noise measurement system, these phase fluctuations between the emitted and received signals are then decomposed in the Fourier frequency domain to create spectral estimates of vibration-induced modulation of the return signal. The goal is to obtain standoff vibration sensitivity that is sufficient to characterize the presence of an unknown or unexpected material that might be internal to the standoff object. The I/Q modulator shown in Fig. 1 is used to calibrate the sensitivity of the phase detector (PD).

III. EXPERIMENTAL RESULTS

The photograph of the set up for determining the sensitivity of the mm-wave vibrometer is shown in Fig. 2. We used a custom varactor-tuned W-band source that can be tuned from 89 to 96 GHz; for this experiment, we used 95 GHz. For a proof-of-concept experiment, we measured the displacement of the mirror controlled by a piezoelectric (PZT) actuator instead of using an actual microwave-induced TAI target. As we could not move the mirror fast enough to test
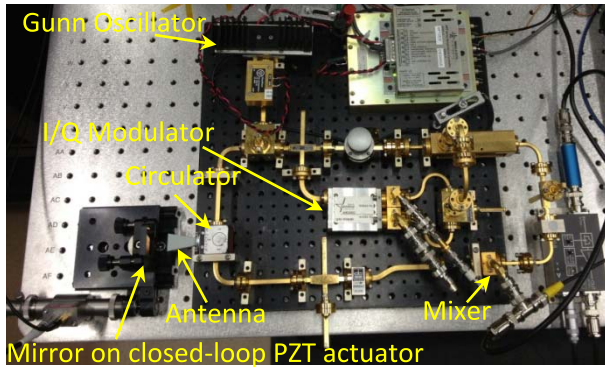
Fig. 2. Experimental realization of the single-channel *W*-band stand-off vibrometer. Here, the target is a mirror on closed-loop PZT actuator. A *W*-band Gunn oscillator with DSB noise, $S_{\varphi-\mathrm{Gunn}}(f) = +77 f^{-3}$ dBrad^2/Hz at 95 GHz is used as the reference carrier and a feedhorn antenna with 20-dB gain is used.
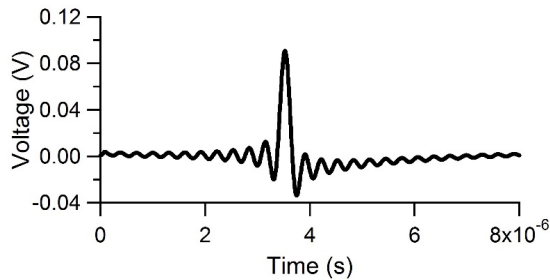

Fig. 3. Phase modulated sinc-shaped pulse used for driving the PZT actuator. The PRF of the sinc-pulse is 100 kHz.

the vibrometer at the frequencies of interest, we generated a phase modulation pulse that simulates a displacement. We used a sinc-shaped pulse at a 100-kHz pulse repetition frequency (PRF), this driving signal is shown in Fig. 3.

For this experiment, the distance between the antenna and the mirror was approximately 2 cm. This distance can be increased by matching the path-length delay between the signals arriving at the LO and RF ports of the mixer. The direct signal and the reflected signal off the mirror were mixed in the PD and the baseband IF signal was processed. For IF processing, we used 80 dB of gain after the mixer and a peripheral component interconnect (PCI) extensions for instrumentation-based field-programmable gate array (FPGA) digitizer sampled at 250 MHz, with 16-bit resolution. In addition, an analog 10-MHz antialiasing low-pass filter, digital bandpass from 10 kHz to 10 MHz, and triggered synchronous averaging of 10k–500k pulses were used for processing. The vibrometer breadboard was mounted on the optical table with vibration-isolating Sorbothane feet. The mechanical coupling of undesired vibration from the actuator into the vibrometer through the baseplate was tested for by substituting the circulator and the antenna with a straight waveguide section and no significant coupling was observed. The amplitude of the sinc-shaped signal was adjusted to produce mirror displacements of 10, 1, and 0.1 nm and measured by the vibrometer. The voltage fluctuations at the output of the PD were measured and the results are depicted in Fig. 4(a)–(c). These results show that the single-channel vibrometer can successfully detect surface displacement of 1 nm. In addition, weak signals can be seen down to approximately 0.2 nm with higher averaging.
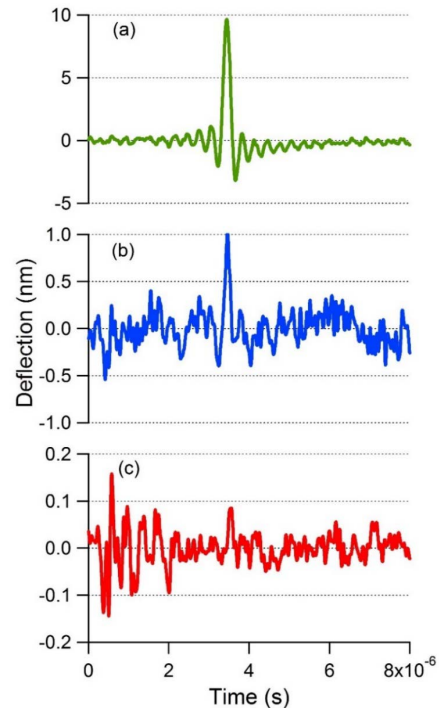

Fig. 4. Detection of the 100-kHz sinc-pulse mimicking a displacement pulse by the *W*-band vibrometer. Different mirror displacement and pulse averaging were used. (a) 10 nm, 10k averages. (b) 1 nm, 10k averages. (c) 0.1 nm, 500k averages.
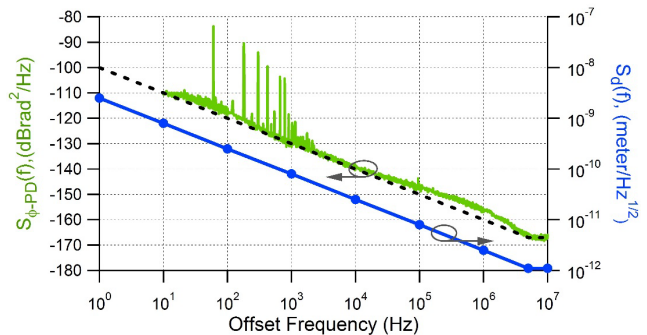

Fig. 5. Plot of the DSB phase noise of the PD at 95 GHz and the corresponding PSD of the displacement.

IV. EFFECT OF PHASE NOISE

The successful realization of applications such as concealed weapons/explosive detection depends on the phase-noise of key components, i.e., mixer, reference oscillator, and other electronics at *W*-band. In this section, we discuss the effect of phase noise of the mixer and oscillator on the vibrometer's sensitivity and maximum range.

A. Sensitivity and Stability

The vibrometer's sensitivity to thermoacoustic signals depends on the residual phase noise of the mixer and also on the signal-to-noise ratio (SNR) of the received signal. The double sideband (DSB) residual phase noise, $S_{\varphi-\mathrm{PD}}(f)$, of the PD and the corresponding power spectral density (PSD) of displacement, $S_d(f)$, calculated from (1) are also shown in Fig. 5. It shows that the displacement measurement is dependent on the flicker phase noise of the PD. To measure displacement
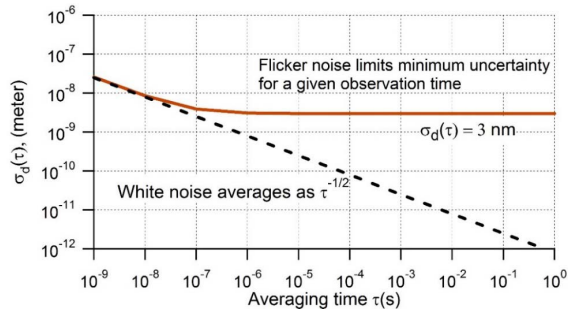
Fig. 6. Displacement measurement uncertainty versus observation time due to the residual phase noise of the PD.

Fig. 7. Block diagram of the two-channel W-band standoff vibrometer. The signal input to ports "x" and "y" is the same as that of Fig. 1.

Fig. 8. Phase noise floor of the W-band (92–96 GHz) measurement system and the corresponding PSD of the displacement.

below 1 nm, a phase noise level below -120 dBrad^2/Hz is needed.

The uncertainty in the displacement measurement, $\sigma_d(\tau)$, due to the flicker-phase and white-phase noise of the PD is shown in Fig. 6. This plot shows that observation of a single measurement longer than 1 μs or (sampling/filtering below 1 MHz) will not result in any further improvement. This is because unlike white noise, the flicker noise does not converge to a mean of zero due to averaging. Therefore, the single channel vibrometer using this PD, the displacement measurement uncertainty is limited to 3 nm. The estimate is calculated from the residual phase noise floor of the measurement system operating at full receive power.

B. Maximum Target Range

If the vibrometer is used without the path-length delay equalized it would act as a frequency discriminator on the driving source and the maximum target range would depend on the phase noise of the W-band source. The free-running oscillator that was used has DSB phase noise, $S_{\varphi-\text{Gunn}}(f) = +77 f^{-3}$ dBrad^2/Hz at 95 GHz. The characterization of the single-channel W-band vibrometer revealed that the free-running Gunn oscillator's frequency modulation (FM) noise was limiting the maximum target range to 5 cm. The FM noise on the Gunn source is converted to residual phase noise at the baseband by

$$S_{\varphi}(f) = S_{\varphi-\text{Gunn}}(f)\left[4\sin^2\left(\frac{4\pi R f}{c}\right)\right] \qquad (2)$$

where c is the speed of light. From initial testing, the thermoacoustic signature of the detected target will most likely reside below a 100-kHz offset frequency. To support the factor of 10 improvements in range and sensitivity, the phase noise of the W-band source must be improved by at least 50 dB between these offset frequencies. We have already shown in [15] and [16] that a scheme for low-phase noise synthesis at W-band can be used here.

V. TECHNIQUE TO INCREASE SENSITIVITY

The single-channel W-band vibrometer discussed above exhibits nanometer-scale sensitivity. While a single measurement longer than 1 μs is limited to 3 nm by the flicker noise of the mixer, synchronous averaging of repetitive signals allows sensitivity down to about 0.2 nm. When a synchronization signal is not available, further improvement to the W-band system
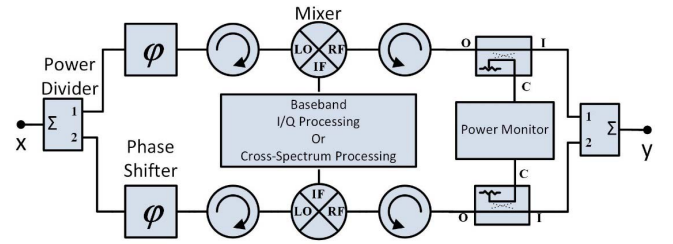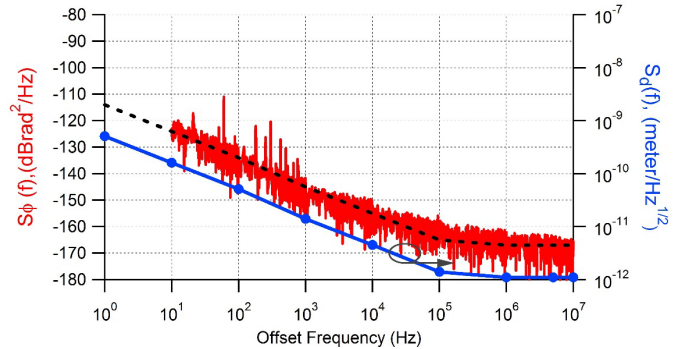
could make it possible to successfully detect subnanometer displacements by adding a second receive channel (Fig. 7). With two independent measurement channels, cross correlation processing [17] of the thermoacoustic signals will give a $\sqrt{N}$ improvement in the receive's SNR, where N is the number of cross correlation averages.

In [15], we reported the performance of a two-channel W-band phase noise measurement system. The phase noise floor of that system is shown as red curve in Fig. 8. The flicker noise floor is almost 15 dB lower than the single-channel system (Fig. 5). If we use this two-channel system as a thermoacoustic vibrometer, it will improve the sensitivity by a factor of 5.

VI. CONCLUSION

We reported a single-channel standoff W-band vibrometer with a sensitivity of 1 nm to thermoacoustic signals. Unlike optical detection, the mm-wave detection scheme demonstrated here can easily infiltrate opaque surfaces and does not require an optically reflective surface of the target. This is, however, at the expense of sensitivity and resolution. In the future, we plan to improve the sensitivity of the vibrometer for the detection of thermoacoustic signals and increase target range by implementing a two-channel system and low-phase-noise oscillator.

REFERENCES

[1] T. Bowen, R. L. Nasoni, A. E. Pifer, and G. H. Sembrosk, "Some experimental results on the thermoacoustic imaging of tissue equivalent phantom materials," in *Proc. IEEE Ultrason. Symp.*, Oct. 1981, pp. 823–827.

[2] Y. Cui, C. Yuan, and Z. Ji, "A review of microwave-induced thermoacoustic imaging: Excitation source, data acquisition system and biomedical applications," *J. Innov. Opt. Health Sci.*, vol. 10, no. 4, 2017, Art. no. 1730007.

[3] A. D. Droitcour, "Non-contact measurement of heart and respiration rates with single chip microwave Doppler radar," Ph.D. dissertation, Stanford Univ., Stanford, CA, USA, 2006.

[4] L. E. Larsen and J. H. Jacobi, Eds., *Medical Applications of Microwave Imaging*. Piscataway, NJ, USA: IEEE Press, 1986.

[5] M. W. Laschke *et al.*, "High-resolution ultrasound imaging: A novel technique for the noninvasive *in vivo* analysis of endometriotic lesion and cyst formation in small animal models," *Amer. J. Pathol.*, vol. 176, no. 2, pp. 585–593, 2010.

[6] S. Bakhtiari, N. Gopalsami, T. W. Elmer, and A. C. Raptis, "Millimeter wave sensor for far-field standoff vibrometry," in *Proc. AIP Conf.*, 2009, vol. 1096, no. 1, pp. 1641–1648.

[7] L. V. Wang and S. Hu, "Photoacoustic tomography: *In Vivo* imaging from organelles to organs," *Science*, vol. 335, no. 6075, pp. 1458–1462, 2012.

[8] A. Hochreiner, J. Bauer-Marschallinger, P. Burgholzer, B. Jakoby, and T. Berer, "Non-contact photoacoustic imaging using a fiber based interferometer with optical amplification," *Biomed. Opt. Express*, vol. 4, no. 11, pp. 2322–2331, 2013.

[9] M. Johansmann, G. Siegmund, and M. Pineda, "Targeting the limits of laser Doppler vibrometry," in *Proc. IDEMA*, Tokyo, Japan, 2005, pp. 1–12.

[10] Y. Qin, P. Ingram, X. Wang, T. Qin, H. Xin, and R. S. Witte, "Non-contact thermoacoustic imaging based on laser and microwave vibrometry," in *Proc. IEEE Int. Ultrason. Symp.*, Chicago, IL, USA, Sep. 2014, pp. 1033–1036.

[11] H. Nan *et al.*, "Non-contact thermoacoustic detection of embedded targets using airborne-capacitive micromachined ultrasonic transducers," *Appl. Phys. Lett.*, vol. 106, pp. 084101-1–084101-4, Feb. 2015.

[12] G. Alexopoulos, K. C. Boyle, N. Dolatsha, H. Nan, B. T. Khuri-Yakub, and A. Arbabian, "Standoff tracking of medical interventional devices using non-contact microwave thermoacoustic detection," in *IEEE MTT-S Int. Microw. Symp. (IMS) Dig.*, San Francisco, CA, USA, May 2016, pp. 1–4.

[13] X. Wang, Y. Qin, R. S. Witte, and H. Xin, "Modeling of non-contact thermoacoustic imaging," in *Proc. USNC-URSI Radio Sci. Meeting (Joint AP-S Symp.)*, Vancouver, BC, Canada, Jul. 2015, p. 314.

[14] X. Wang, T. Qin, Y. Qin, A. H. Abdelrahman, R. S. Witte, and H. Xin, "Microwave-induced thermoacoustic imaging for embedded explosives detection in high-water content medium," *IEEE Trans. Antennas Propag.*, to be published.

[15] A. Hati, C. W. Nelson, and D. A. Howe, "PM noise measurement at W-band," *IEEE Trans. Ultrason., Ferroelectr., Freq. Control*, vol. 61, no. 12, pp. 1961–1966, Dec. 2014.

[16] T. M. Fortier *et al.*, "Optically referenced broadband electronic synthesizer with 15 digits of resolution," *Laser Photon. Rev.*, vol. 10, no. 5, pp. 780–790, Sep. 2016.

[17] W. F. Walls, "Cross-correlation phase noise measurements," in *Proc. IEEE Freq. Control Symp.*, May 1992, pp. 257–261.